Numerical Analysis of the Flow and Heat Transfer Characteristics for Forced Convection-Radiation in Entrance Region of an Internally Finned Tubes

Hi-Yong Pak*, Kyoung-Woo Park and Moon-Suk Choi*****

(Received April 18, 1997)

The flow and heat transfer characteristics of combined forced convection and radiation in the entrance region of internally finned tubes are investigated numerically in this paper. The uniform flow is considered for an inlet flow condition. A three dimensional parabolic problem is solved by a marching-type procedure envolving a series of two dimensional elliptic problems in the cross-stream plane. The SIMPLER-algorithm and Raithby's pressure-velocity coupling method are employed to analyze the flow and heat transfer characteristics. For the calculation of radiative heat transfer, the P_1-approximation and the weighted sum of gray gases method (WSGGM) are used. The effects of fin height, number of fins, optical thickness, reference temperature, and Planck number on the flow and heat transfer characteristics are examined. It was found that the effect of fin-height on the heat transfer characteristic is more dominant than that of number of fins. The present results show that the optimal non-dimensional fin height and number of fins are 0.4 and 16, respectively.

Key Words: Numerical Analysis, Internally Finned Tube, Force Convection-Radiation, Marching Scheme, P_1-Approximation, WSGGM

Nomenclature

a : Radius of tube $(=D_i/2)$, [m]
c_p : Specific heat at constant pressure, $[J\text{kg}^{-1}\ K^{-1}]$
D_e : Equivalent hydraulic diameter, [m]
D_i : Inner diameter of tube, [m]
D_o : Outer diameter of tube, [m]
f : Friction factor
G : Total irradiation, $[W\text{m}^{-2}]$
G^* : Dimensionless total irradiation
H : Fin height, [m]
h : Dimensionless fin height $(=H/D_i)$
k_r : Conductivity ratio of fluid to solid $(=k_s/k_f)$
N : Number of fins
Nu : Nusselt number
P' : Dimensionless cross-sectional excess pressure
$\bar{P}$: Dimensionless cross-sectional average pressure
p' : Cross-sectional excess pressure, [Pa]
$\bar{p}$: Cross-sectional average pressure, [Pa]
Pl : Planck number
Pr : Prandtl number
$\bar{q}$: Average heat flux, [W m^{-2}]
$\vec{q}_r$: Radiation flux vector
R : Dimensionless radial coordinate
r : Radial coordinate, [m]
Re : Reynolds number
T_{in} : Temperature of inlet fluid, [K]
T_w : Wall temperature, [K]
U : Dimensionless velocity for θ-coordinate
u : Velocity for θ-coordinate, $[m\ s^{-1}]$
V : Dimensionless velocity for r-coordinate
v : Velocity for r-coordinate, $[m\ s^{-1}]$

* Department of Mechanical Engineering, Hanyang University, Seoul, 133-791, Korea
** Building System Research Lab., LGIS Co., Ltd., Incheon, 402-200, Korea
*** Graduate Student, Hanyang University, Seoul, 133-791, Korea

W : Dimensionless velocity for z-direction
w : Velocity for z-direction, [$m\ s^{-1}$]
Z : Dimensionless axial coordinate
z : Axial coordinate, [m]

Greek symbols

θ : Angular coordinate, [rad]
Θ : Dimensionless temperature
Θ_b : Dimensionless bulk temperature
Θ_{ref} : Dimensionless reference temperature
μ : Viscosity, [$kg\ m^{-1}\ s^{-1}$]
ν : Kinematic viscosity, [$m^2\ s^{-1}$]
ρ : Density, [kg m^{-3}]
σ : Stefan-Boltzmann constant, [$W\ m^{-2}\ s^{-4}$]
τ : Optical thickness

1. Introduction

Recently, there have been many researches on how to efficiently harness the energy of high temperature gas being emitted from the industrial factories. Among many ways to extract the energy which is not used and left in the combustion gas, the most practical way is installing a heat exchanger that has a fin inside the tube at the outlet region of the system. Therefore, the heat exchanger design of high-efficiency and optimization is necessary and a more accurate analysis of the flow and heat transfer characteristics inside the tube is needed.

There have been many experimental and analytical researches on the pressure drop and heat transfer characteristics of the internally finned tubes. Most of the analytical studies are limited to the case of a fully developed flow or convection only. For the heat exchanger of a combustion system, the radiation effect must not be neglected. So the combined effects of convection and gas radiation must be considered simultaneously for the accurate and optimal design of a heat exchanger.

Most previous numerical and experimental investigations for the laminar flow and the heat transfer in internally finned circular tubes have dealt exclusively with the radiation effect. Rustum and Soliman (1988) took into account of the effect of secondary flow in the tube with internal fins on the heat transfer of laminar mixed convection flow. In considering the thickness and conductivity of fins and tube, the effect of the fin conductivity ratio on the heat transfer for the fully developed inlet flow was performed by Kettner et al. (1991). They reported that the Nusselt numbers for two values of k_f/k_s, i. e. 0.1 and 0.01, were 5% and 10% lower, respectively, than that for $k_f/k_s=0$. Prakash and Liu (1985a. 1985b) studied the process of flow and heat transfer for the uniform inlet velocity, and showed that the heat transfer was improved about 140% for $h=0.6$(fin height). Pak et al. (1996) studied the flow and heat transfer characteristics for the two different inlet conditions, the fully developed and uniform velocity, and showed the heat transfer was improved about 300% in the case of uniform velocity.

Recently, combined convection and radiation analyses have been performed for the internally finned tubes. Morales et al. (1991) studied the combined convection and gray gas radiation in longitudinally finned tubes. They presented the effect of the optical thickness on the bulk temperature, and the most active heat transfer occurred when the optical thickness was 1. Seo et al. (1994) analyzed the effect of non-gray radiation and convection for a simultaneously developing flow in the entrance region under the assumption of 100% fin efficiency(i. e. $k_f/k_s=0$). They said that the heat transfer(Nusselt number) in finned tubes was very efficient for $N=12$ and $H=0.3$.

From the above literature review, it was found that a number of studies considered only the convective heat transfer, whereas a few studies have been performed with gas radiation for internally finned tubes. Furthermore, most researches ignored the effects of conductivity and thickness of the fin.

In this paper, the combined convection and radiation in internally finned tubes with non-gray combustion gas is analyzed numerically. The effects of Planck number, temperature ratio of the inlet fluid to the tube wall, and the conductivity ratio of the fin to the fluid on the flow and heat transfer characteristics are investigated numerically. The effects of the fin numbers and the

height on the heat transfer are also studied.

2. Numerical Modeling

2.1 Geometric configuration and basic assumptions

Figure 1 shows the internally finned circular tube under consideration in this study. It consists of a circular tube of inner diameter(D_i) with a number of longitudinal fins. The fins and tube have some thickness and conductivity. Therefore the geometry is defined by four parameters: number of fins(N), fin heights(H), fin thickness(t), and conductivity of fin and tube(k).

This analysis is applicable to a steady, laminar, incompressible flow forced convection and gas radiation, Newtonian fluid with constant properties. Viscous dissipation and axial conduction within the fluid are assumed to be negligible. The working fluid is a mixture of carbon dioxide, water vapor, and nitrogen($Y_{CO_2}=0.08$, $Y_{H_2O}=0.16$, $Y_{N_2}=0.76$), which is a typical combustion gas for simulation. The optical thickness of non-gray gas is obtained by using the weighted-sum-of-gray-gases model(Smith et al., 1982), which varies with temperature. The conductivity of fin and tube is assumed to be constant, and the outside tube wall is maintained at low temperature. The flow is assumed to be developing with uniform inlet velocity and high temperature.

2.2 Governing equations and boundary conditions

In the present study, the flow is assumed to have a predominant direction, the horizontal z-direction, so it is treated as a parabolic flow

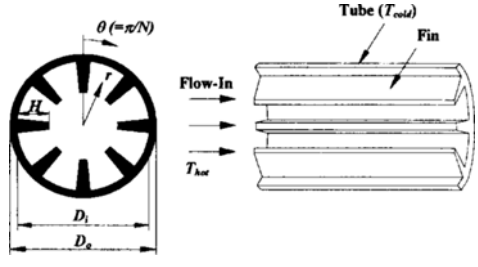

Fig. 1 Schematic diagram of internally finned circular tube.

where the diffusion of mass, momentum, and energy along the axial direction can be neglected. Also, along the axial direction, downstream pressure has no effect on the flow conditions of upstream. This parabolic assumption implies that the pressure can be written as,

$$p(r,\theta,z)=\bar{p}(z)+p'(r,\theta) \tag{1}$$

where $\bar{p}(z)$ represents an average pressure over the cross section and $p'(r,\theta)$ is the pressure variation in the cross stream plane. The axial velocity(W) is driven by the gradient of $\bar{p}(d\bar{p}/dz)$, while the velocities of r, θ-direction of cylindrical coordinate (V, U) are generated by the gradient of $p'(\partial p'/\partial r)$ and, $p'(\partial p'/\partial\theta)$, respectively. From these, the three-dimensional parabolic internal flow problem is solved by a parabolized Navier-Stokes procedure, that is, employing a marching-type computational procedure.

Using the assumption expressed by relation (1), the continuity, momentum and energy equations can be expressed in the following dimensionless forms:

Continuity:

$$\frac{1}{R}\frac{\partial}{\partial R}(RV)+\frac{1}{R}\frac{\partial U}{\partial\theta}+\frac{\partial W}{\partial Z}=0 \tag{2}$$

r-momentum:

$$V\frac{\partial V}{\partial R}+\frac{U}{R}\frac{\partial V}{\partial\theta}+W\frac{\partial V}{\partial Z}=-\frac{\partial P'}{\partial R}+\frac{1}{R}\frac{\partial}{\partial R}\left(R\frac{\partial V}{\partial R}\right)+\frac{1}{R^2}\frac{\partial^2 V}{\partial\theta^2}+\frac{U^2}{R}-\frac{V}{R^2}-\frac{2}{R^2}\frac{\partial U}{\partial\theta} \tag{3}$$

θ-momentum:

$$V\frac{\partial V}{\partial R}+\frac{U}{R}\frac{\partial V}{\partial\theta}+W\frac{\partial U}{\partial Z}=-\frac{1}{R}\frac{\partial P'}{\partial\theta}+\frac{1}{R}\frac{\partial}{\partial R}\left(R\frac{\partial U}{\partial R}\right)+\frac{1}{R^2}\frac{\partial^2 U}{\partial\theta^2}-\frac{UV}{R}+\frac{2}{R^2}\frac{\partial V}{\partial\theta}-\frac{U}{R^2} \tag{4}$$

z-momentum:

$$V\frac{\partial W}{\partial R}+\frac{U}{R}\frac{\partial W}{\partial\theta}+W\frac{\partial W}{\partial Z}=-\frac{\partial\bar{P}}{\partial Z}+\frac{1}{R}\frac{\partial}{\partial R}\left(R\frac{\partial W}{\partial R}\right)+\frac{1}{R^2}\frac{\partial^2 W}{\partial\theta^2} \tag{5}$$

Energy:

$$V\frac{\partial\Theta}{\partial R}+\frac{U}{R}\frac{\partial\Theta}{\partial\theta}+W\frac{\partial\Theta}{\partial Z}=\frac{1}{\mathrm{Pr}}\left\{\frac{1}{R}\frac{\partial}{\partial R}\left(\frac{\partial\Theta}{\partial R}\right)\right.$$

$$+\frac{1}{R^2}\frac{\partial^2\Theta}{\partial\theta^2}\Big\}+\frac{4}{\mathbf{Pr}\cdot Pl}\tau[G^*-\pi(\Theta+\Theta_{ref})^4] \quad (6)$$

Conduction in fin and tube:

$$\frac{k_r}{\mathrm{Pr}}\Big\{\frac{1}{R}\frac{\partial}{\partial R}\Big(R\frac{\partial\Theta}{\partial R}\Big)+\frac{1}{R^2}\frac{\partial^2\Theta}{\partial\theta^2}\Big\}=0 \quad (7)$$

Overall mass conservation:

$$\iint_{duct}\rho W dA=\dot{m}=constant\ for\ z\text{-}direction \quad (8)$$

A new term, G^*, appears in the energy Eq. (6). This term represents a nondimensional radiative intensity which is obtained by solving the radiative transport equation (RTE). For calculating the radiation intensity, spherical harmonics approximation (Menguic, 1985) (P_1) is adopted in this study. The nondimensional form of the radiative transport equation for the radiative intensity is written as follows (Ozisik, 1973):

$$\frac{\partial}{\partial R}\Big(R\frac{\partial G^*}{\partial R}\Big)+\frac{1}{R^2}\frac{\partial^2 G^*}{\partial\theta^2}=3\tau^2[G^*-\pi(\Theta+\Theta_{ref})^4] \quad (9)$$

The radiative intensity at the wall is determined by using the Marshark's boundary condition (Ozisik, 1973). The boundary conditions for RTE are given by

$$\frac{\partial G^*}{\partial n}=-\frac{3}{2}\tau[G^*-\pi(\Theta+\Theta_{ref})^4] \quad at\ rigid\ wall \quad (10a)$$

$$\frac{\partial G^*}{\partial n}=0 \quad at\ symmetric \quad (10b)$$

where n is the normal direction.

The governing Eqs. (2) ~ (9) are nondimensionalized by introducing the following dimensionless parameters:

$$R=\frac{r}{a},\ Z=\frac{z}{a\mathrm{Re}},\ V=\frac{va}{\nu},\ U=\frac{ua}{\nu},$$
$$W=\frac{w}{\bar{w}},\ \bar{P}=\frac{\bar{p}}{\rho\bar{w}^2},\ P'=\frac{p'a^2}{\rho\nu^2},$$
$$\Theta=\frac{T-T_w}{T_{in}-T_w},\ \Theta_{ref}=\frac{T_w}{T_{in}-T_w},\ \mathrm{Re}=\frac{\bar{w}a}{\nu},$$
$$\mathrm{Pr}=\frac{\mu C_p}{k_f},\ Pl=\frac{k_f/a}{\sigma(T_{in}-T_w)^3},$$
$$G^*=\frac{G}{4\sigma(T_{in}-T_w)^4} \quad (11)$$

where Pl, means the Planck number which is defined by the ratio of radiation to conduction and represents the radius of tube ($=D_i/2$)

The boundary conditions to solve the governing equations are as follows:

(1) inlet ($Z=0$):
$$U=0,\ V=0,\ W=W_{in},\ \Theta=\Theta_{in} \quad (12a)$$

(2) outside wall:
$$\Theta=\Theta_{wall} \quad (12b)$$

(3) symmetric surface:
$$\Big(\frac{\partial\phi}{\partial R}\Big)_{\theta=0}=\Big(\frac{\partial\phi}{\partial R}\Big)_{\theta=\pi/N}=0,\ (\phi=V,\ W,\ \Theta) \quad (12c)$$
$$\Big(\frac{\partial\phi}{\partial\theta}\Big)_{R=0}=0,\ (\phi=U,\ W,\ \Theta) \quad (12d)$$
$$U_{\theta=0,\pi/N}=0,\ V_{R=0}=0 \quad (12e)$$

(4) contact surface with fluid and solid:
$$U=V=W=0 \quad (12f)$$
$$k_r\Big(\frac{\partial\Theta}{\partial n}\Big)_{solid}=\Big(\frac{\partial\Theta}{\partial n}\Big)_{fluid}-\frac{\Theta_{ref}}{Pl}\vec{G}^* \quad (12g)$$

where n is a unit dimensionless distance in the normal direction of contact surface.

2.3 Numerical analysis

Governing Eqs. (2) ~ (9) were solved numerically using a control volume-based finite difference method. The three dimensional parabolic problem was solved by the marching type procedure envolving a series of two dimensional elliptic problem in the cross-stream plane. The marching step size is 5×10^{-4} along the axial distance. At each marching step, the strong coupling of pressure and velocity in the cross section was calculated by the SIMPLER-algorithm (Patankar, 1980). Axial pressure and velocity were solved by Raithby's parabolic pressure-velocity coupling method (Raithby and Schneider, 1979).

The computations were performed on a non-uniform grid in the cross-stream plane ($r-\theta$ coordinates); the grid lines were closely packed near the fin and tube.

The P_1-approximation was applied to solve the radiative transport equation, which was very useful to solve the problem of coupling radiation and flow field. The working fluid was assumed to be a combustion gas which is a non-gray participating gas. The properties of the working fluid, such as absorption coefficient or optical

thickness, were obtained by using the weighted sum of gray-gases model (Raithby and Schneider, 1979). In this model, the participating band is divided into several sub-bands and the optical thickness of each sub-band was assumed to be a constant.

The discretized equations by a control volume based finite difference method were calculated iteratively by using the line-by-line TDMA. To avoid the numerical divergence and to promote the convergence, under-relaxation method was adopted. Convergence was assumed to be achieved when the changes in all velocity components and the temperatures at all grid point were within $\pm 10^{-5}$, and the residual of the continuity equation at all mesh points was within 10^{-5}.

3. Results and discussion

In this study, the effects of geometric variation and radiation heat transfer on the flow and thermal characteristics at the entrance region are investigated numerically in the internally finned circular tube. The flow is assumed to be develop ing hydrodynamically and thermally with uniform inlet velocity and constant high temperature. The emissivity of the tube and fins is assumed 1.0.

The ranges of geometrical parameters and flow conditions in this study are given in Table 1.

Grid dependence: The choice of adequate grid system is very important for the accurate analysis because there are many symmetric planes in this computational domain. Three types of the grid system (30×15, 40×20, and 50×30) are considered for the standard conditions; $Pl=0.2$, $h=0,4$, $N=16$, $\Theta_{ref}=1$ and $k_r=100$. In this study, the grid dependence is verified by comparing the Nusselt numbers for three grid systems. The circumferentially averaged Nusselt number is determined by

$$Nu=\frac{\bar{q}\cdot D_e}{k(\Theta_w-\Theta_b)} \tag{13}$$

where $\bar{q}$ is the average heat flux and Θ_b is the bulk temperature at any cross section is obtained as follows:

$$\Theta_b=\frac{\int w\Theta\cdot rdrd\theta}{\int w\cdot rdrd\theta} \tag{14}$$

where the integrals are performed over the cross section of the tube.

Figure 2 shows the Nusselt number variations with axial distance for the three grid systems. Nusselt number is calculated from Eq. (13). Figure 2 indicates that the Nusselt number for 30×15 grid system is 16% and 71.7% lower than for 50×30 system around the upstream and the downstream, respectively. While the Nusselt number for 40×20 system is lower than that of 50×30 system by 8% (upstream) and 17.3% (downstream), respectively. The computational time for 30×15, 40×20, and 50×30 grid system was 2, 3. 5, and 6 hours (based on the 586-Pentium PC, 150Mhz), respectively. For comparatively small error and computational time, the 40×20 grid system is adopted in this study.

Table 1 Parameters for this study.

● ***Fluid***	
1) Radiation effect	- considered, neglected
2) Planck number	- 0.2, 0.5
3) Optical thickness	- 1, 2, and calculated
4) Temperature ratio	- 1, 2
● ***Geometery***	
1) Fin height	- smooth tube, 0.2, 0.4, 0.6, 0.8
2) Number of fins	- 4, 8, 12, 16, 20
3) Conductivity ratio	- 100

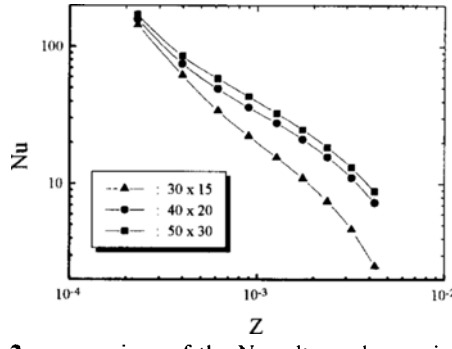

Fig. 2 comparison of the Nusselt number variation for three types of grid system at standard conditions.

3.1 Flow characteristics

The hydrodynamic phenomenon is generally explained by the pressure drop due to friction along the axial distance. Let $d\bar{p}/dz$ be the local pressure gradient at some axial location. The relation between pressure drop and the value can be presented as follows:

$$f = -\frac{\frac{d\bar{p}}{dz}\cdot\frac{D_e}{4}}{\rho\cdot\frac{w^2}{2}} = -0.5\cdot\frac{1}{\mathrm{Re}}\frac{dP}{dZ} \qquad (15)$$

Here, f represents a local friction factor, Re is Reynolds number ($=\bar{w}a/v$) and D_e is the equivalent hydraulic diameter defined as follows:

$$D_e = \frac{2\cdot a}{(Nh/\pi+1)} \qquad (16)$$

where h is the dimensionless fin height (H/a).

Figure 3 depicts the pressure drop as a function of axial distance (z) in the internally finned tube for several different numbers of fin, Fig. 3(a), and several fin heights, Fig. 3(b). In each cases, the fin height and the number of fins is fixed as 0.4 and 16, respectively. As shown in Fig. 3, the pressure drop decreases dramatically at the entrance region and decreases slowly along the developing region down to the fully developed value. Finally, the pressure drop becomes a constant value for all cases (as the axial distance is over 0.1). Figure 3(a) shows that the pressure drop is large as the number of fins increases. But the difference is not so big. This is attributed to the fact that the secondary flow occurrs at the central region of tube rather than the fin surroundings. Therefore, in the case of a relatively low fin height, h=0.4, the effect of number of fins on the pressure drop is little. Figure 3(b) shows that the pressure drop ($f\cdot$Re) increases as the fin height increases. Particularly, for the case of h=0.6 and h=0.8, $f\cdot$Re increases rapidly in comparison with the case of h=0.4, because the fins are concentrated at the central part of tube and then the flow of this region is disturbed by the fins. It can also be seen that the difference of pressure drop for the variation of fin heights in comparison with that of number of fins, Fig. 3(a), is large because the flow disturbance by the increased fin height at the central region of tube is generated more vividly.

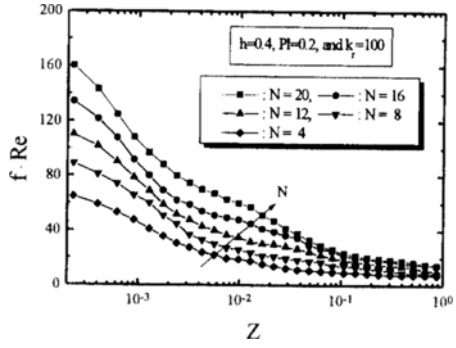

(a) Effect of number of fins

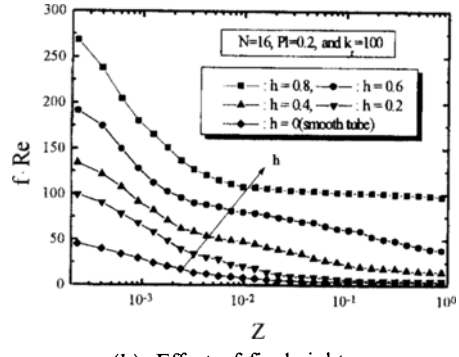

(b) Effect of fin heights

Fig. 3 Pressure drop with the axial distance for various (a) number of fins and (b) fin heights.

3.2 The effect of radiation parameters

Figure 4 represents the axial variation of bulk temperature (Θ_b) for the pure (τ=0) and com-

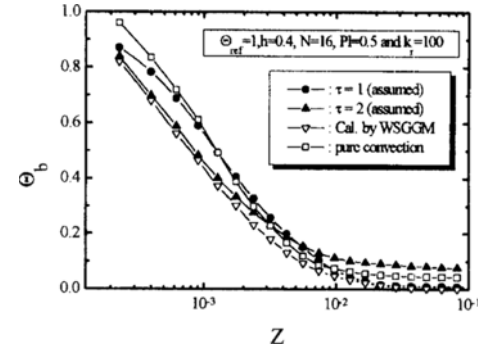

Fig. 4 Bulk temperature variation with the axial distance for several optical thickness at Θ_{ref} =1.0, Pl=0.5, h=0,4, N=16, and k_r=100.

bined convection (i. e. $\tau=1$, 2, and calculated by WSGGM) at $\Theta_{ref}=1.0$, $Pl=0.5$, $h=0.4$, $N=16$, and $k_r=100$. The optical thickness (τ) is defined as the multiplication of absorption coefficient and characteristic length, it means the amount of extinction energy while the radiative energy passes the medium. The bulk temperature for radiation is lower than that of the pure convection case. It means that the heat transfer (or Nusselt number) with the radiation is greater than that for the pure convection. For the assumed (fixed) optical thickness, such as $\tau=1$ and 2 in Fig. 4, as the optical thickness increases, the heat transfer increases at near the inlet. On the contrary, at the downstream ($Z\geq0.005$), the heat transfer decreases. This is due to the fact that the amount of heat absorbed by working fluid with larger optical thickness at downstream is increased . It means that the cooling is occurred slowly in the tubes (that is, the cooling length is increased) as the optical thickness becomes large. But, by using WSGGM, both of the fluid temperature and the optical thickness are decreased at the downstream. Therefore, it is not appropriate to assume that optical thickness is constant (or fixed), because the optical thickness varies with fluid temperature. The results indicate that the case of $\tau=2$ provides similar result as WSGGM at upstream and the case of $\tau=1$ provides similar result as WSGGM at downstream, respectively.

Cooling length for various conditions are presented in Table 2. Cooling length is very important factor for the optimization of tube length. In this study, cooling length is defined as the length at which the bulk temperature decreases below 0.1, i. e., the length when the thermal energy of inlet fluid is recovered more than 90%. Table 2 shows that the cooling length with radiation by using the WSGGM is shorter than that with pure convection and constant optical thickness. Hence, in order to calculate the radiative heat transfer when the bulk temperature varies with the axial distance, it is essential to estimate the optical thickness by using WSGGM.

Figure 5 illustrates that the bulk temperature for the two different temperature ratios and the Planck numbers varies with the axial distance.

Table 2 Cooling length for various optical thickness.

Optical thickness		Cooling length
Pure convection ($\tau=0$)		0.0062
Assumed or fixed	$\tau=1$	0.0120
	$\tau=2$	0.0250
Calculated by WSGGM		0.0048

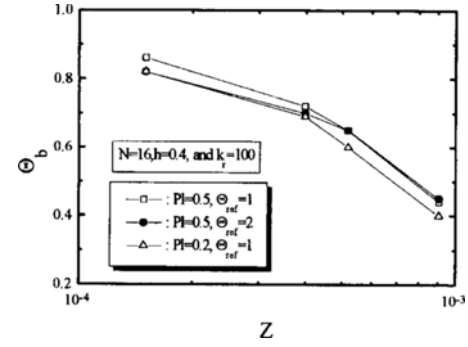

Fig. 5 Bulk temperature variation with the axial distance for two different temperature ratio and Planck numbers.

The bulk temperatures for $\Theta_{ref}=2$, $Pl=0.5$ and $\Theta_{ref}=1$, $Pl=0.2$ decrease more rapidly than the case of $\Theta_{ref}=1$, $Pl=0.5$. That is, as radiation effect is more dominant in the flow and thermal fields (i. e., Planck number changes from 0.5 to 0. 2), radiation heat transfer is increased which affects the bulk temperature decreasing. However, the convection heat transfer remains constant even though the temperature ratio is changed.

3.3 The effect of geometric parameters

In order to optimize the finned tube, the pressure drop and the heat transfer are considered simultaneously. However, the excessive pressure drop occurred when the fin height is over 0.4 (see Fig. 3). Therefore, the two cases of fin height ($h=0.2$ and 0.4) are considered.

Figure 6 shows the temperature contours for different fin heights ($h=0.2$, 0.4) and numbers of fin ($N=16$, 20) at two points of axial distance ($z=0.0004$, 0.004). The maximum temperature at $z=0.0004$ is 0.98 and 0.96 for the cases of $h=0.2$, $N=16$ and $h=0.4$, $N=20$, respectively. In the

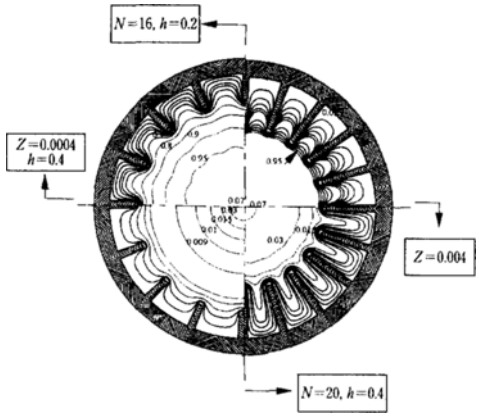

Fig. 6 Isotherms for the number of fins and fin heights at different axial location.

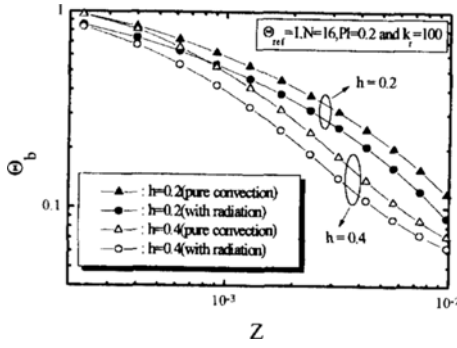

Fig. 7 Effect of fin height on the bulk temperature in cases of pure convection and combined convection-radiation at $\Theta_{ref}=1.0$, $N=16$, $Pl=0.2$, and $k_r=100$.

meantime, the maximum temperature at $z=0.004$ is 0.084 and 0.078 for the same conditions as mentioned above. Thus, it was found that the heat transfer is enhanced as the number of fin and fin height are increased simultaneously, and that the flow and thermal fields are more rapidly developed.

The effect of fin height on the bulk temperature for pure convection and combined convection -radiation at $N=16$, $Pl=0.2$, and $k_r=100$ is shown in Fig. 7. As the height of fin increases from 0.2 to 0.4, the bulk temperature decreases rapidly(i. e. the heat transfer increases). In the case of pure convection, the bulk temperature for $h=0.4$ is 3.2% and 45.0% lower than that for $h=0.2$ at $z=0.0004$ and 0.0042, respectively. When

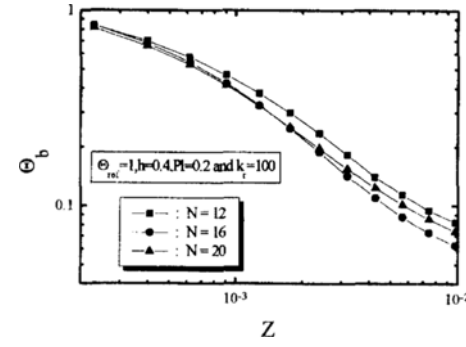

Fig. 8 Effect of number of fin on the bulk temperature for the case with radiation at $\Theta_{ref}=1.0$, $h=0.4$, $Pl=0.2$, and $k_r=100$.

radiation is considered, the difference of bulk temperature for the two cases($h=0.2$ and 0.4) becomes large for the same locations. Especially, it was found that the effect of fin height on the thermal characteristics at downstream is more important than at upstream. At upstream, the effect of radiation is more dominant because the temperature difference between working fluid and tube wall is large. It can also be seen that the bulk temperature with considering the effect of radiation is lower than that for the pure convection under the same fin height. This means that for the case with radiation the heat transfer rate increases owing to the rapid thermal development.

Figure 8 shows the bulk temperature variation with the axial distance for various numbers of fin ($N=12$, 16, and 20) at $h=0.4$, $Pl=0.2$, and $k_r=100$. The bulk temperature decreases as the number of fins increases, because the heat transfer rate increases due to the extension of heat transfer area. However, the bulk temperature for $N=20$ becomes higher than that for $N=16$ over $z=0.0025$. That is, the bulk temperatures for $N=16$ and $N=20$ are 3.1% and 5.8% lower, respectively, than that for $N=12$ at $z=0.0004$. For the axial location of $z=0.0042$, the bulk temperature difference is 21.6% and 11.9%, respectively, for the same conditions as mentioned above. This is due to the significant reduction of velocity and the weakness of convection in the space between the two consecutive fins. This phenomenon becomes more pronounced at downstream. Therefore, it is not necessary to increase the number of fins over 16

Table 3 Cooling length for the various gemetric parameters in the cases with and without radiation.

Geometric parameters		Cooling length	
No. of fins (N)	Fin height (h)	With radiation	Without
12	0.2	0.0105	0.0121
	0.4	0.0061	0.0076
16	0.2	0.0089	0.0114
	0.4	0.0048	0.0062
20	0.2	0.0091	0.0116
	0.4	0.0057	0.0073

for the enhancement of heat transfer because the heat transfer rate is not proportional to the number of fins.

Table 3 shows the cooling length for various geometric parameters in the cases with and without radiation. As shown in Table 3, cooling length with the radiation is 13% to 23% shorter than that without radiation. This is due to the increase of radiation effect. It means that the effect of radiation on the thermal characteristics is very strong and the influence of convection becomes weak with the increases of the fin height and number of fins .

As mentioned earlier, there is little increase in the bulk temperature when the number of fins is greater than 16, and the fin height is more significant parameter over the number of fins for pressure drop and heat transfer enhancement. The present results also show that the optimal number of fins and fin height is 16 and 0.4, respectively, in the cases considered in this study.

4. Conclusions

Combined forced convection and radiation for non-gray gas at the entrance region of internally finned circular tube is analyzed numerically. A three dimensional parabolic problem is solved by a marching-type procedure envolving a series of two dimensional elliptic problem in the cross sectional plane. For the calculation of radiative heat transfer and optical thickness of non-gray gas, P_1-approximation and WSGGM are adopted, respectively. The effects of radiation, fin height, number of fins on the flow and heat transfer characteristics are investigated by considering the fin thickness and conductivity.

It was found that WSGGM has to be used to obtain the optical thickness because the bulk temperature varies with the axial distance. When the fin height (h) is increased more than 0.6, there is a significant pressure drop. When the number of fins (N) is greater than 16, there is little enhancement of heat transfer. The results also show that the optimal fin height and number of fins are 0.4 and 16, respectively, in the present work.

References

(1) Rustum, I. M. and Soliman, H. M., 1988, "Numerical Analysis of Laminar Forced Convection in the Entrance Region of Tubes with Longitudinal Internal Fins," *ASME J. of Heat Transfer*, Vol. 110, pp. 310~313.

(2) Ketter, I. J., Degani, D., and Gutfinger, C., 1991, "Numerical Study of Laminar Heat Transfer in Internally Finned Tubes," *Numerical Heat Transfer*, Part A, Vol. 20, pp. 159~180.

(3) Prakash, C. and Liu, Y. D., 1985a, "Analysis of Laminar Flow and Heat Transfer in the Entrance Region of an Internally Finned Circular Duct," *ASME J. of Heat Transfer*, Vol. 107, pp. 84~91.

(4) Prakash, C. and Liu, Y. D., 1985b, "Buoyancy Induced Flow in a Vertical Internally Finned Circular Duct," *ASME J. of Heat Transfer*, Vol. 107, pp. 119~123.

(5) Pak, H. Y., Park, K. W., and Choi, M. S., 1996, "A Numerical Study on the Heat Transfer Characteristics in an Internally Finned Circular Tube Flow," *J. of Air Conditioning and Refrigeration* (in Korean), Vol. 8, No. 2, pp. 267~278.

(6) Molales, J. C., Campo, A. and Schuler, C., 1991, "Heat Transfer Enhancement in Internally Finned Tubes Accounting for Combined Convection and Participating Radiation," *Int. J. of Heat ans Mass Transfer*, Vol. 34, No. 7, pp. 1861~1869.

(7) Seo, T., Jensen, M. K. and Kaminski, D. A., 1994, "Combined Convection and Radiation in Simultaneously Developing Flow and Heat Transfer in Internally Finned Tubes with Non -Gray Gas Mixture," *10th Int. Heat Transfer Conference*, Vol. 2, pp. 135~140.

(8) Smith, T. F., Shen, Z. F. and Friedman, J. N., 1982, "Evaluation of Coefficients for the Weighted Sum of Gray Gases Model," *ASME J. of Heat Transfer*, Vol. 104, pp. 602~608.

(9) Menguic, M. P. 1985, "Modeling of Radiative Heat Transfer in Multi- Dimensional Enclosures Using Spherical Harmonics Approximation," Ph. D. Thsiss, Purdue Univ.

(10) Ozisik, M. N., 1973, *Radiative Transfer and Interaction with Conduction and Convection*, John-Wiley and Sons, Co., New York.

(11) Patankar, S. V., 1980, *Numerical Heat Transfer and Fluid Flow*, Hemisphere, Washington, D. C.

(12) Raithby, G. D. and Schneider, G. E., 1979, "Numerical Solution of problems in Incompressible Fluid Flow-Treatment of the Velocity -Pressure Coupling," *Numerical Heat Transfer*, Vol. 2, pp. 417~440.